一体成型泡沫铝夹芯双管的抗落锤冲击性能

许心沛¹, 张赞², 丁俭¹*, 崔李鹏¹, 邱子轩¹, 李泳¹, 陈朋崴¹, 张子晨³*, 刘泊霄¹, 夏兴川¹* (1河北工业大学, 天津 300130; 2邢台学院, 河北 邢台 054001; 3苏州实验室, 江苏 苏州 215100)
*通讯作者: 夏兴川, 男, 研究员, 博士 E-mail: xiaxingchuan0101@163.com; 丁俭, 女, 副教授, 博士 E-mail: djian0122@126.com; 张子晨, 男, 博士 E-mail: zhangzc@szlab.ac.cn

摘 要:泡沫填充管是一种优异的能量吸收结构。本文采用改进的熔体发泡方法原位制备了泡沫铝夹芯双管(IFAFSDTs),实现了泡沫铝芯和内外铝合金管的冶金结合。研究表明,保温温度对冶金结合质量至关重要,最佳温度为410℃。通过落锤冲击试验系统研究了直径比(R)和长径比(L)对力学性能和能量吸收性能的影响。结果表明,承载能力和能量吸收性能随着R或L的增加先增后降。当R和L较大时IFAFSDTs表现出更稳定的载荷波动和形变加速度。外管变形模式呈现轴对称圆环屈曲,内管呈现非对称钻石型屈曲。泡沫芯的能量吸收机制主要包括孔结构变形与坍塌、晶粒变形及晶界断裂。由于泡沫芯不同区域的变形程度不同,微观结构呈现显著变化,各区域的主导吸能模式存在差异。

关键词:一体成型泡沫铝夹芯管;冶金结合;轴向抗冲击性能;能量吸收

Drop-Weight Impact Resistances of Integrated Forming Aluminum Foam Sandwich Double Tubes

XU Xin-pei¹, ZHANG Zan², DING Jian^{1,*}, CUI Li-peng¹, QIU Zi-xuan¹, LI Yong¹, CHEN Peng-wei¹, ZHANG Zi-chen^{3,*}, LIU Bo-xiao¹, XIA Xing-chuan^{1,*}

(1.School of Material Science and Engineering, Hebei University of Technology, Tianjin, 300130, PR China; 2.School of Physics and Electronic Engineering, Xingtai University, Xingtai 054001, PR China; 3.Suzhou Laboratory, Suzhou 215100, PR China.)

Abstract: Aluminum foam filled tubes are good energy-absorbing structures. In this paper, integrated forming aluminum foam sandwich double tubes (IFAFSDTs) were fabricated utilizing an improved melt foaming method to achieve metallurgical bonding between aluminum foam core and inner/outer aluminum alloy tubes. Results indicated that holding temperature is crucial for the metallurgical bonding and the optimal holding temperature is 410 °C. The mechanical properties and energy absorption performance of IFAFSDTs were investigated through drop-weight impact tests, with specific focusing on the effect of diameter ratio (R) and aspect ratio (L). The load-carrying capacity and energy absorption performance increase first and then decrease with the increase of R or L. IFAFSDTs with high values of R and L exhibit relatively stable load fluctuations and deformation acceleration during the impact process. The outer tube undergoes an axisymmetric circular ring symmetric buckling mode, while the inner tube exhibits an asymmetric diamond mode. Energy absorption modes of aluminum foam core include pore structure deformation and collapse, grain deformation and intergranular fracture. Due to the different extent of deformation in different regions of the aluminum foam core, the dominant energy absorption mode in each region changes and the microstructure after impact shows obvious differences.

Keywords:Integrated forming aluminum foam sandwich double tubes (IFAFSDTs); metallurgical bonding; axial impact resistance; energy absorption.

1. Introduction

Aluminum foam, characterized by low density, high strength, excellent energy absorption capacity and stable deformation modes, is extensively utilized in the field of energy absorption and shock mitigation ^[1, 2]. However, due to inferior mechanical properties of cell walls in surface layer of aluminum foam and its inadequate surface quality, it is commonly utilized as a filling material ^[3].

Aluminum foam-filled tubes (FFTs) represent a typical composite structure, characterized by solid metal outer layer and an aluminum foam core [4, 5]. Due to the inherent advantages of aluminum foam and solid metal tubes, as well as their synergistic interaction, the yield strength and deformation stability of FFTs are significantly improved, exhibit exceptional energy absorption performance and load carrying capabilities [6, ^{7]}. However, its specific energy absorption falls short compared to that of the corresponding hollow tubes [8, 9]. Therefore, in order to further enhance energy absorption efficiency and mechanical properties of FFTs, novel composite structure aluminum foam sandwich double tubes (AFSDTs) were proposed [10, 11]. This structure generally comprises inner and outer layers of solid metal, as well as a middle layer of aluminum foam core. Researches have demonstrated that the component under this combination exhibit a significant improvement of overall crashworthiness and energy absorption efficiency compared to those of both the double hollow tubes and the single tube filled with metal foams [12, 13]. Consequently, it represents an efficient and stable energy absorption component with significant potential for impact protection applications.

AFSDTs can be fabricated through two typical methods: secondary processing method and integral forming technique. The secondary processing method involves initially cutting aluminum foam and solid metal tubes to the required dimensions, followed by bonding the two components using adhesives, brazing, or mechanical fastening. This method is characterized by its straightforward fabrication principle and is currently the most widely employed approach for producing aluminum structures [14]. However, foam-filled aluminum foam-filled structures fabricated via the secondary processing method often exhibit several limitations, including low interfacial bonding strength, high density and susceptibility to damage during processing [15, 16]. The integral forming method enables the simultaneous achievement of foam formation in aluminum foam core and the metallurgical bonding at the interface between aluminum foam core and solid metal tubes [17]. The strength of the metallurgical bonding at the interfacial layer significantly influences the mechanical properties of aluminum foam-filled structures [18, 19]. Consequently, the melt foaming method holds substantial potential for the production of AFSDTs. However, the preparation of AFSDTs using melt foaming method is considerably challenging due to the confined foaming space within

AFSDTs and the limited heat dissipation conditions of the inner tube.

Previous studies have demonstrated that inner and outer tubes of AFSDTs play a crucial role in guiding and controlling the deformation of metal foam core, thereby optimizing its impact energy absorption capacity [20, 21]. The foam core significantly improves the overall energy absorption performance of this structure, with the magnitude of this enhancement being dependent on the filling density [22]. Foam-filled sandwich double tubes exhibit superior energy absorption characteristics and deformation resistance when compared to single-tube counterparts [23, 24]. Furthermore, the height of the aluminum foam-filled structure has been identified as a critical factor influencing load fluctuation and energy absorption capacity [25]. Despite these advancements, the majority of research investigating the mechanical properties of AFSDTs has predominantly focused on specimens fabricated through secondary processing methods. Limited attention has been given to the impact resistance of AFSDTs manufactured via integral forming processes. Notably, these AFSDTs featuring metallurgical bonding interfaces present substantial potential for applications in energy absorption and buffering systems.

In this study, an improved melt foaming method was employed to fabricate integrated forming aluminum foam sandwich double tubes (IFAFSDTs) with varying heights and inner tube diameters. The influence of holding temperature on metallurgical bonding between aluminum foam core and inner/outer aluminum alloy tubes was systematically studied. Through axial drop weight impact tests, the effects of diameter ratio (R) and aspect ratio (L)on the axial impact resistance and energy absorption performance of IFAFSDTs were evaluated. By comparing the experimental results of FFTs fabricated by other methods, it has been confirmed that IFAFSDTs have superior impact resistance and energy absorption capabilities. Deformation modes and failure mechanisms of IFAFSDTs during axial impact process were thoroughly investigated through detailed analysis of their deformation processes. The energy absorption mechanism of IFAFSDTs during the impact process is analyzed.

2 Materials and methods

2.1 Specimen preparation

IFAFSDTs were fabricated using an improved melt foaming method. 6063 aluminum alloy tubes were selected as inner/outer tubes. Industrial pure aluminum

ingots (Al, with purity of 99.5 wt.%), magnesium ingots (wetting agent, with purity of 99.5 wt.%), calcium (thickening agent, commercially granularity between 1.0 and 2.5 mm), and TiH₂ powders (foaming agent, commercially pure, 300±20 mesh) were used to prepare aluminum foam core. The specific preparation process is as follows: (1) heating and melting a certain amount of pure aluminum at 690 °C; (2) adding about 1wt.% Mg into the melt then stirring for 4 min under speed of 400 r/min; (3) adding about 2 wt.% Ca particles and stirring for 6 min under speed of 400 r/min; (4) adding 1.5 wt.% TiH₂ and stirring rapidly for 10 seconds under the speed of 1200 r/min; (5) pouring foaming melt into the gap of inner and outer tubes, then taking out the mold and cooling it to room temperature.

The metallurgical bonding between aluminum foam core and tubes is crucial for the overall structural strength and impact resistance ^[26]. In order to achieve metallurgical bonding, the effect of holding temperature (330°C, 370°C, 410°C, 450°C and 490°C) on metallurgical bonding of interface was investigated with the foaming stirring temperature fixed at 690°C.

To systematically investigate the effect of diameter ratios (R) and aspect ratios (L) on impact resistance, IFAFSDTs with diameter of 60 mm, various R and L were fabricated. For a fixed height of 60 mm, inner tube

diameters of 27 mm, 21 mm and 15 mm corresponded to R of 0.45, 0.35 and 0.25. For a fixed inner tube diameter of 27 mm, sample heights of 60 mm, 75 mm, and 90 mm corresponded to L of 1, 1.25, and 1.5, respectively. For each set of parameters, three samples were prepared to ensure reproducibility of experiments and the average values were used.

2.2 Pore structure analysis

To accurately characterize the pore size distribution, porosity and circularity of IFAFSDTs, the pore structure in both cross-sectional and longitudinal-sectional were comprehensively analyzed. Images of the horizontal and vertical symmetry planes of IFAFSDTs were selected and processed using Image J software for binarization, as illustrated in Figure 1. By statistically evaluating the pore structural characteristics within regions 1, 2a and 2b, and applying Equation (1)-(3) for calculation, the overall pore size distribution D_E , porosity P_E and circularity C_E of IFAFSDTs were determined. D_1 , D_{2a} and D_{2b} represent the distribution frequency of pore sizes in regions 1, 2a and 2b, respectively. P_1 , P_{2a} , P_{2b} and C_1 , C_{2a} , C_{2b} denote the average porosity and average circularity within these three regions.

$$D_E = D_1 \times 50\% + (D_{2a} + D_{2b}) \times 50\% \tag{1}$$

$$P_E = P_1 \times 50\% + (P_{2a} + P_{2b}) \times 50\% \tag{2}$$

$$C_E = C_1 \times 50\% + (C_{2a} + C_{2b}) \times 50\%$$
 (3)

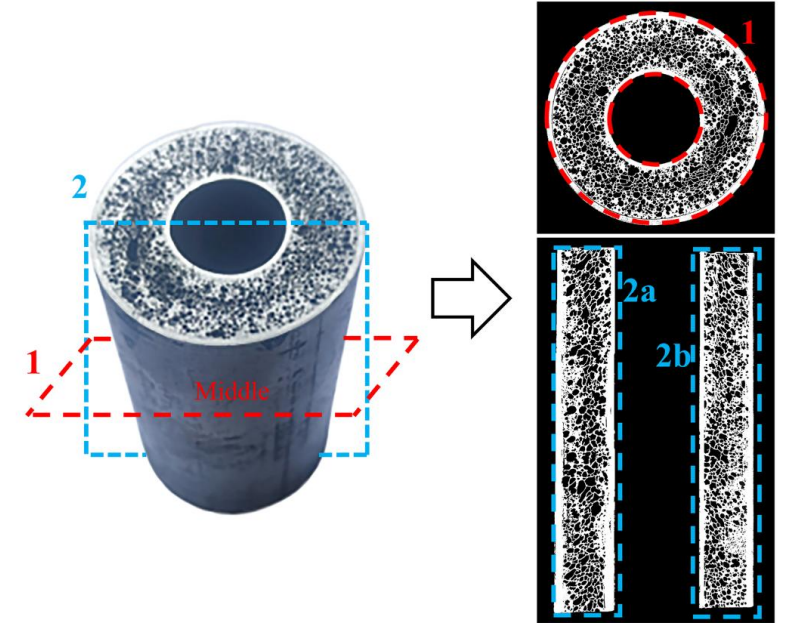


Figure 1 Statistical method for pore structure.

2.3 Drop weight impact test

Drop weight impact tests were conducted to investigate the axial impact resistance of IFAFSDTs. Related testing system and method have been reported in authors' previous research ^[27]. The impact body consisted of drop hammer and counterweight, with a total mass of 104.7 kg, which was fixed at initial position with vertical height of 4 m. The impact force, impact action time and vertical

deformation displacement were recorded during drop-weight impact test. In addition, several key parameters were selected for further evaluating the axial impact resistance performance of IFAFSDTs. Peak crushing force (PCF) is the first peak stress in impact force-displacement curve. Total energy absorption (EA) can be expressed by Equation (4) [28]:

$$EA = \int_0^\delta F(x) dx \tag{4}$$

where x is axial compression displacement of sample after impact body contacts IFAFSDTs, δ represents the maximum displacement and F(x) represents the impact force on the specimen when axial displacement is x. In addition, energy absorption capacity (W) represents the energy absorption per unit volume of the specimen, which can be calculated by Equation (5) [29]:

$$W = \int_0^{\tau} \sigma(\varepsilon) d\varepsilon \tag{5}$$

where ε is axial compression strain of sample, τ represents the maximum strain and $\sigma(\varepsilon)$ represents the stress value when strain is ε . Besides, mean crushing force (MCF) is the ratio of total energy absorption to effective impact deformation displacement, as shown in Equation (6) [30]:

$$MCF = \frac{EA}{\delta} \tag{6}$$

Peak stress and mean stress can be obtained by dividing the PCF and MCF by the stress area of the specimen. Then undulation of load-carrying capacity (ULC) is the ratio of the work done by the specimen deviating from the MCF during the impact process to the total energy absorption and reflects the amplitude of impact force variation of the specimen in test process [31], which can be calculated by Equation (7). A lower ULC value indicates a reduced amplitude of load fluctuations.

$$ULC = \frac{\int_0^{\delta} |F(x) - MCF| dx}{EA}$$
 (7)

2.4 Finite element simulation

Finite element (FE) simulation of the drop-weight impact process of IFAFSDTs was conducted using ABAQUS software. The FE model consists of IFAFSDT, drop hammer, and support panel, as shown in Figure 2. The model of IFAFSDT is obtained by reconstructing micro-CT scanning images (Sanying Precision Instruments Co., Ltd., China, Tianjin) using Avizo software (Thermo Fisher Scientific, USA, Tianjin

Sanying Precision Instrument Co., Ltd.). The Johnson-Cook model is used to describe the deformation behaviour of the matrix alloy Al-Ca-Ti Mg. Assuming that the alloy hardens isotropically, without considering true strain and temperature, the relationship between flow stress σ and equivalent plastic strain ε can be expressed as:

$$\sigma = (A + B\varepsilon^n)(1 + C\ln\dot{\varepsilon}^*) \tag{8}$$

where \mathcal{E}^* is the dimensionless strain rate, A is the yield strength, B and n are strain hardening coefficients, C presents the strain rate sensitivity coefficient. Specific constitutive parameters were obtained by substituting experimental data into the solution and are listed in table 1.

Table 1. Constitutive parameters of Johnson-Cook model of Al-Ca-Ti Mg alloy

A/MPa	B/Mpa	n	С
82.354	153.4968	0.5650	0.0049

In ABAQUS, the contact interaction between hammer and sample, the contact between sample and support are set as surface-to-surface contact. The contact caused by the deformation and collapse of cell walls is set as self-contact. The bottom of sample is bound to support by rigid body constraint. The impact process is simulated by dynamic/explicit modules, and the impact load is simulated by applying an initial velocity to the hammer through a predefined velocity field.

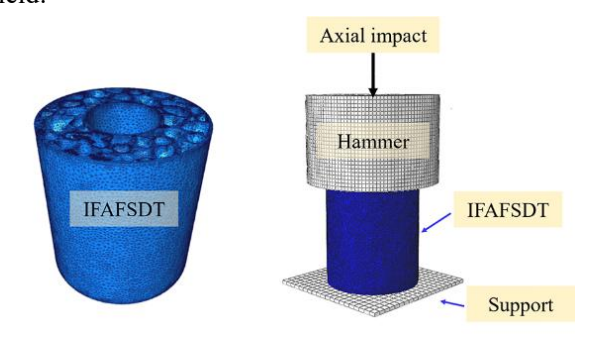


Figure 2 FE model of drop-weight impact process on IFAFSDTs

3. Results and discussion

3.1 Interface metallurgical bonding situation

The holding temperature is important for the metallurgical bonding of the interface between aluminum foam core and inner/outer tubes. Figure 3 shows the interface bonding of IFAFSDTs prepared at holding temperatures of 330 °C, 370 °C, 410 °C, 450 °C and 490 °C.

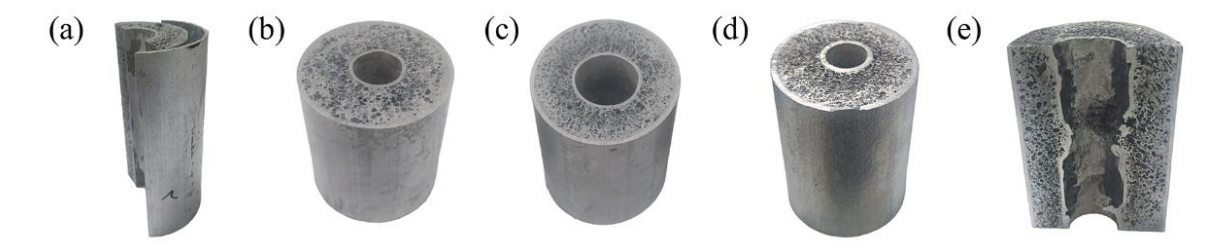


Figure 3 Influence of holding temperature on combination of interface: (a) 330 ℃; (b) 370 ℃; (c) 410 ℃; (d) 450 ℃; (e) 490 ℃.

the holding temperature was 330 °C, metallurgical bonding between aluminum foam core and outer tube was not realized. The solidification of aluminum foam melt was too fast under low holding temperature, resulting in a low porosity of aluminum foam core and lots of solid regions in the core layer. When holding temperature rose to 370 °C, although the macroscopic combination of aluminum foam core and inner/outer tubes was achieved, there still existed a clear boundary according to the SEM images (Figure 4). This is attributed to the low holding temperature which caused the melt in contact with the wall of aluminum alloy tube to solidify rapidly and hindered the metallurgical bonding at the interface. Moreover, the porosity of the specimen was low and the pore size in the bottom region of IFAFSDTs was small. When holding temperature was 410 °C, a good metallurgical bond was achieved according to the SEM images. This is because high-temperature aluminum foam melt has excellent fluidity and can fully wet the wall of aluminum alloy tubes [32]. When holding temperature is relatively high, the mutual diffusion of atoms in melt and in the surface of aluminum tube results in the formation of metallurgical bonding. In addition, the pore size distribution of aluminum foam core is uniform and the wall thickness of cells decreases with increased porosity [33]. Under holding temperature of 450 °C, the metallurgical combination was achieved, but the inner tube locally deformed. Some concentrated large holes appeared in the foam core. When holding temperature reached 490 °C, inner tube was severely deformed. This is because the holding temperature is too high, and the heat dissipation space of inner tube is limited, resulting in

melting and deformation of the inner tube. Besides, the aluminum foam core has more concentrated large holes and the pore size distribution is not uniform. Therefore, a holding temperature of 410 °C is more desirable for the preparation of IFAFSDTs.

Based on BSE image and EDS line scanning results in Figure 5, the interfacial metallurgical bonding was further verified. It is evident that no abrupt changes in elemental contents were observed at the interface. Subsequently, inner/outer aluminum alloy tube were separated from aluminum foam core. As shown in Figure 6, after the IFAFSDTs were separated, aluminum foam debris remained on the wall of the aluminum alloy tube. The above experiments sufficiently demonstrated that the metallurgical combination was formed between the foam aluminum core and inner/outer tubes.

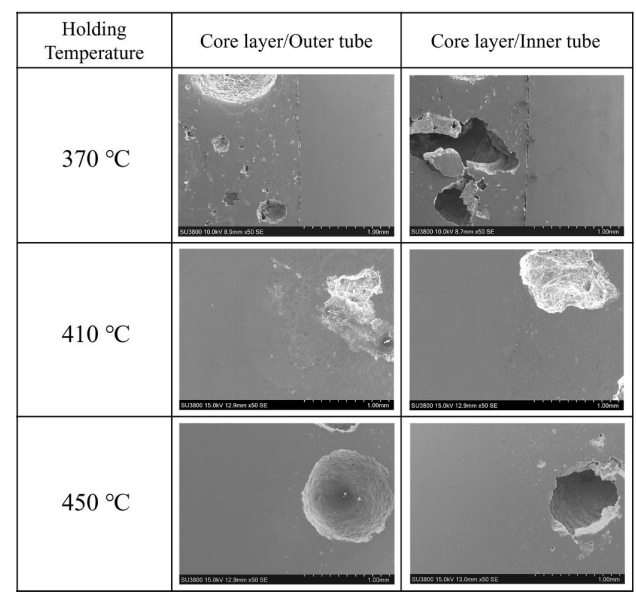


Figure 4 The effect of holding temperature on interface metallurgical bonding

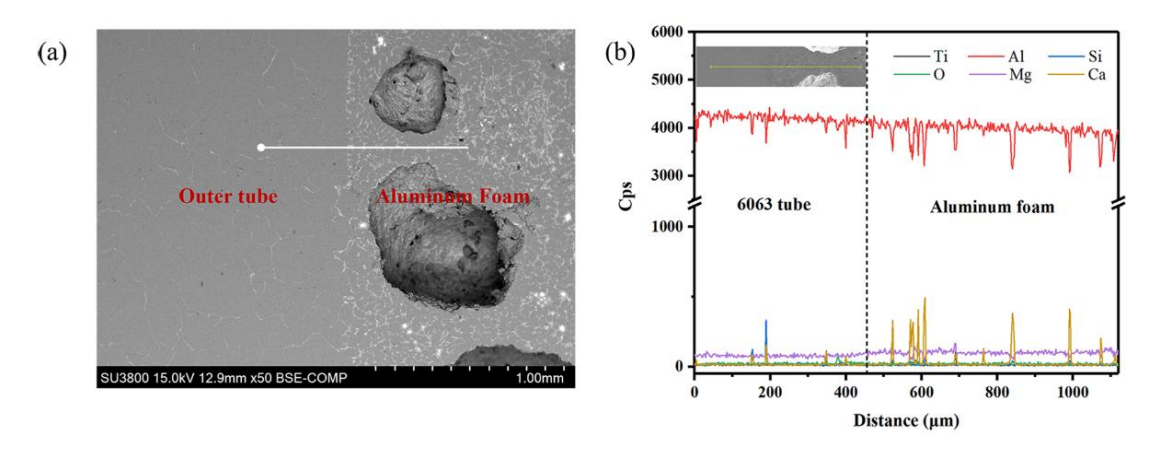


Figure 5 The variation of elements at bonding interface under holding temperature of 410 ℃: (a) BSE image; (b) EDS line scan results.



Figure 6 Interface morphology between aluminum foam core and aluminum alloy tubes after IFAFSDTs were separated: (a) inner tube; (b)(c) outer tube.

3.2 Pore structure

A series of IFAFSDTs were fabricated with holding temperature of 410 °C. Since porosity and pore size significantly influence the mechanical properties of aluminum foam [34, 35], in addition to holding temperature, parameters such as holding time, casting time, and cooling time were also precisely controlled to ensures that the porosity and pore diameter of the sample remain stable.

A typical pore structure distribution is illustrated in Figure 7. The diameter of pores (D) in regions 1, 2a, and 2b, as well as the entire sample, conform to normal distribution, following D \sim N(0.79, 0.71²), N(0.89, 0.90²), $N(0.79, 0.79^2)$ and $N(0.81, 0.76^2)$, respectively. The majority of pore sizes in samples were concentrated in the range of 0.5~1.5 mm, with few concentrated large pores. The porosities in 1, 2a, 2b, and the entire sample were 63.1%, 62.2%, 61.6%, and 62.5%, respectively. The circularities were relatively high and similar in all four statistical regions, with values of 0.82, 0.80, 0.85, and 0.82, respectively, which is beneficial for improving the mechanical properties [36]. Therefore, IFAFSDTs have nearly identical pore structures in both transverse and longitudinal sections. This is because that during the integrated preparation, the temperature in holding and cooling processes was uniform and accurately controlled, allowing bubbles to grow, evolve, and solidify uniformly within the mold cavity. Finally, IFAFSDTs exhibits uniform distribution of pore size, porosity and circularity, with a small average pore size, which is conducive to improving the comprehensive performance [37].

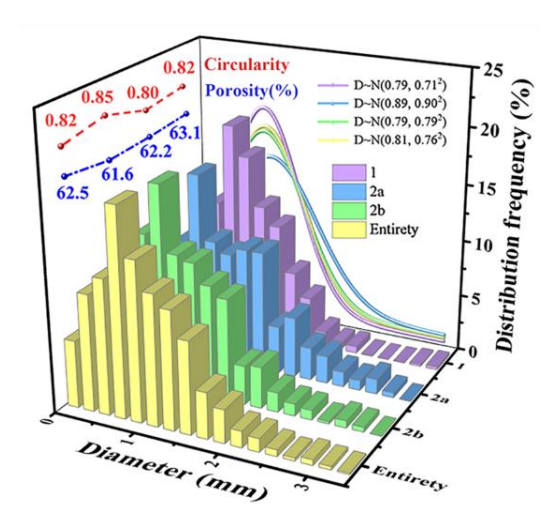


Figure 7 Distribution of pore size, porosity and circularity in regions 1, 2a, 2b and the entire sample

3.3 Effect of diameter ratio on drop weight impact resistance

Figure 8 (a) presents the axial deformation displacement under drop weight impact with R of 0.25, 0.35 and 0.45. As R increases, the axial displacement first decreases and

then increases, indicating that the increase in inner tube diameter and reduction in aluminum foam filling cause the stiffness of IFAFSDTs to first increase and then decrease [38]. Figure 8 (b)-(d) show the force-displacement curves for specimens with varying R. The impact force-displacement curves can be divided into three stages [39, 40]: (1) linear elastic stage: both cell walls of aluminum foam core and inner/outer aluminum tubes undergo elastic deformation, causing the impact force to surge rapidly to a peak; (2) progressive buckling stage: the cell walls and tubes experience plastic deformation, leading to the collapse of the aluminum foam core and buckling of the thin-walled tubes, which in turn causes the impact force to diminish gradually to a lower level; (3) unloading stage: the dissipation of kinetic energy from the impacting body results in a swift decline of the impact force to zero. Observations indicate that

IFAFSDTs, exhibit load fluctuations within a certain range over an extended period when subjected to axial impact, signifying a stable impact resistance mechanism [41]. As R increases, the duration of impact force and vertical deformation displacement in IFAFSDTs initially decreases before ascending, whereas the PCF escalates from 252 kN to 283 kN before descending to 230 kN. Similarly, the MCF increases from 150 kN to 171 kN, then decreases to 137 kN. Given the nearly identical porosities among specimens, the load-bearing capacity of IFAFSDTs is predominantly governed by the inner tube diameter and the volume of aluminum foam filler. Compared with composite aluminum foam filled tubes (CAFTs) without inner tube, the peak load of IFAFSDTs appears later, and the impact force in progressive buckling stage is more stable, which indicates that its load bearing process is more stable [27, 42].

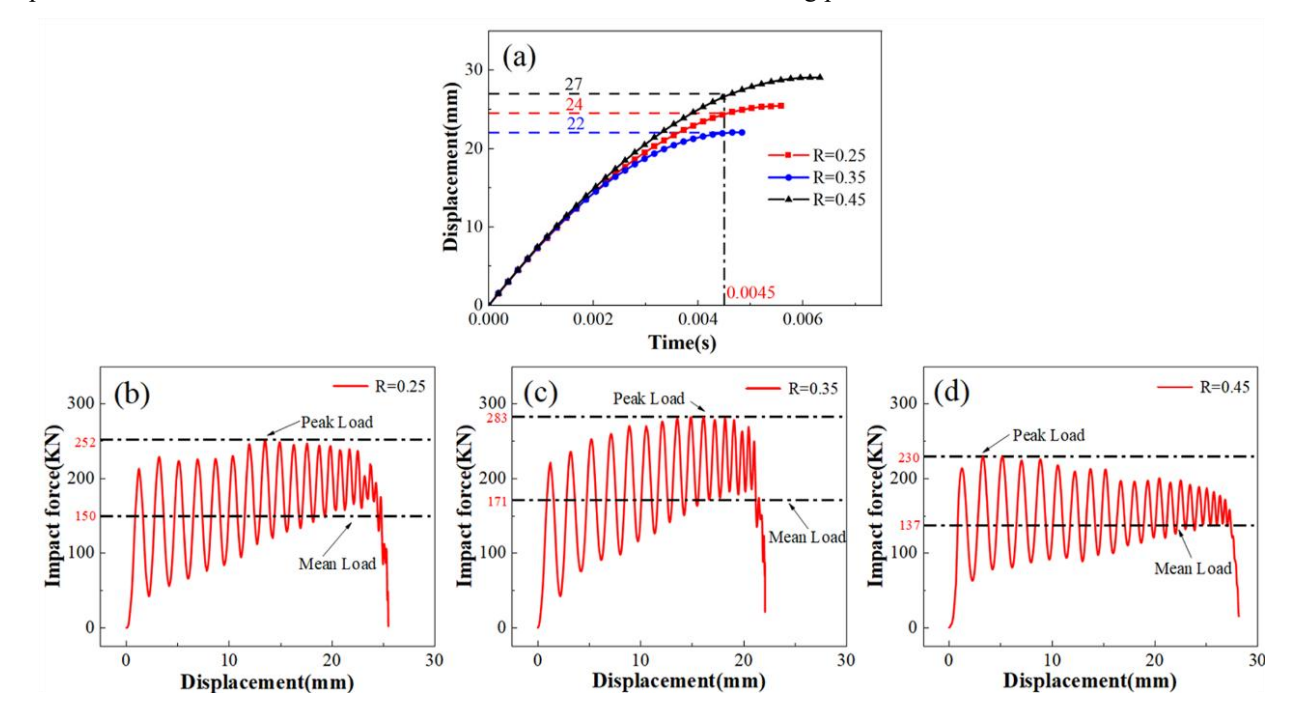


Figure 8 Effect of R on deformation displacement and impact force of IFAFSDTs:

(a) displacement-time curves; (b)-(d) impact force-displacement curves

Figure 9 illustrates the effect of R on both the total absorbed energy and energy absorption capability of IFAFSDTs, respectively. As R increases, the energy absorption performance first increases and then decreases. Under the same deformation displacement and strain, IFAFSDTs with R=0.35 have the highest total energy absorption and energy absorption. With a deformation displacement of 20 mm, the specimens with R=0.25, 0.35

and 0.45 absorbed total impact energies of 2930 J, 3435 J and 2713 J respectively. When strain is 0.3, the energy absorption capacity of the specimens with R=0.25, 0.35 and 0.45 is 33.9 MJ/m³, 43.3 MJ/m³ and 35.8 MJ/m³, respectively. Consequently, IFAFSDTs with R of 0.35 demonstrated the highest PCF, MCF and energy absorption performance, underscoring the superior axial impact resistance.

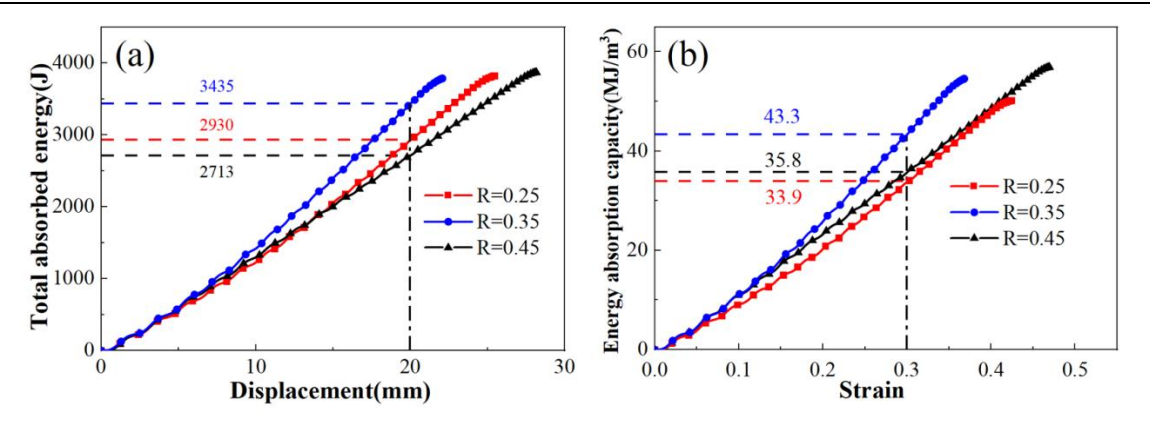


Figure 9 Effect of R on energy absorption performance of IFAFSDTs: (a) total energy absorption; (b) energy absorption capacity.

The crashworthiness of IFAFSDTs can be assessed by load-carrying capacity (ULC), the reduction of deformation velocity and the fluctuation of deformation acceleration [43]. The ULC is a key parameter for evaluating the structural resistance to impact. A smaller value corresponds to a smoother load fluctuation under impact loads [44]. Figure 10 (a) illustrates the effect of R on the ULC of IFAFSDTs. Upon initial contact with hammer, all specimens exhibited obvious fluctuations, representing the primary stage of energy absorption. Meanwhile, aluminum foam core undergoes densification while the aluminum alloy tube forms folds [45]. Subsequently, as the impact process advanced, these load fluctuations gradually diminished. The specimen with R=0.25 exhibited highest ULC value during the impact process, while the load fluctuations curves of the specimens with R=0.35 and 0.45 were lower than those of the specimen with R=0.25. This suggests that increasing the inner tube diameter can enhance the structural load-carrying capacity IFAFSDTs and reduce the degree of load fluctuation during the impact process. The effect of R on the deformation velocity of IFAFSDTs is shown in Figure 10 (b), with vertical deformation displacement of 20.0 mm, the deformation velocity of

three specimens are 4.12 m/s, 2.85 m/s and 5.20 m/s, respectively, which are reduced by 53.4%, 67.8% and 41.2% compared to the initial impact velocity. Specimen with R=0.35 demonstrates superior kinetic energy absorption capacity, effectively reducing the speed of impact bodies. Figure 9 (c) illustrates the effect of R on the deformation acceleration of IFAFSDTs. When subjected to impact, IFAFSDTs experience an initial rapidly increase in acceleration followed by a sustained elevation with fluctuation. Among these samples, the specimen with R of 0.35 exhibits the highest peak acceleration, suggesting superior structural strength [46]. The sample with R of 0.45 demonstrates a consistently lower peak acceleration throughout the impact process. A lower peak acceleration and fluctuation amplitude of crash protection structures can effectively mitigate injuries to personnel or damage to items [47].

In addition, the impact fore fluctuation of IFAFSDTs is smaller than that of CAFTs. Samples of the same size have better deceleration effects under the same deformation displacement. IFAFSDTs have higher deformation acceleration and smoother fluctuations, indicating that IFAFSDTs are better impact protection structures [27].

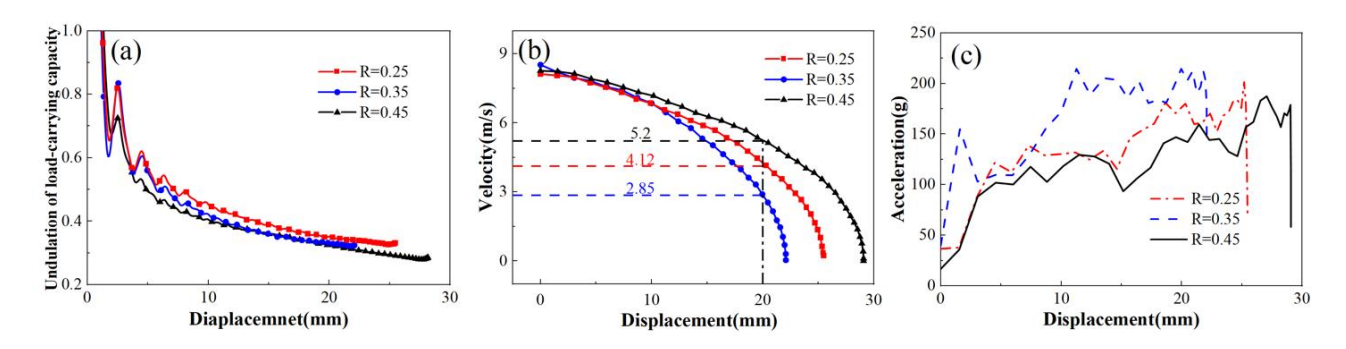


Figure 10. Effect of R on crashworthiness of IFAFSDTs: (a) undulation of load-carrying capacity; (b) deformation velocity; (c) deformation acceleration.

3.4 Effect of aspect ratio on drop weight impact resistance

Figure 11 (a) presents the axial deformation displacement of IFAFSDTs with L of 1, 1.25 and 1.5. The axial displacement decreases first and then increases with the increase of L. This indicates that the stiffness of specimen initially increases and then decreases [48]. The corresponding impact force-displacement curves for specimens with varying L are illustrated in Figure 10 (b)-(d), which still comprise three stages: linear elastic stage, progressive buckling stage and unloading stage. The PCF initially increases from 230 kN to 244 kN, followed by a subsequent reduction to 168 kN with increasing L. Similarly, MCF exhibits an initial rise from 137 kN to 161 kN before decreasing to 103 kN. This behavior suggests that the load-bearing capacity of IFAFSDTs undergoes a gradual enhancement followed by a significant reduction as L increases, under constant geometric and material parameters. This is because IFAFSDTs with relatively low L, the aluminum foam core will enter the densification stage earlier in the process, thereby exhibiting load-carrying performance [14] and inhibiting further deformation of aluminum alloy tubes [49]. As the height increases, the volume of aluminum foam filler increases, and the contact area between the aluminum foam core and the inner/outer aluminum alloy tubes increases, resulting in the enhanced interaction between sandwich

core and aluminum alloy tubes ^[50]. Consequently, within a specific height range, the load-bearing performance continues to improve. However, as the height of the IFAFSDTs increases further, in accordance with Euler's formula for stable load-bearing capacity of tubes in engineering mechanics, longer rods or tubes are more susceptible to buckling or failure under axial loading, as shown in Equation (9):

 $F_{cr} = \frac{\pi^2 EI}{H^2} \tag{9}$

is ultimate bearing capacity before F_{cr} where deformation of tubes, E is elastic modulus. I is the cross-sectional moment of inertia, which is only related to the inner and outer diameters of the tubes, and H is the height of specimen. According to Eq (8), when inner and outer diameters of tubes are constant, the ultimate bearing capacity will decrease with the increase of H before buckling occurs. Moreover, when the height of IFAFSDTs is high, aluminum foam core will not densify earlier during the progressive collapse deformation, reduces the impact of aluminum foam densification on the impact resistance performance, thereby reducing the impact loads [51]. Although the peak and mean stresses of IFAFSDTs with L of 1.5 are significantly lower than those with L of 1 and 1.25, these IFAFSDTs exhibit longer energy-absorbing stroke, representing an effective strategy for improving impact resistance safety.

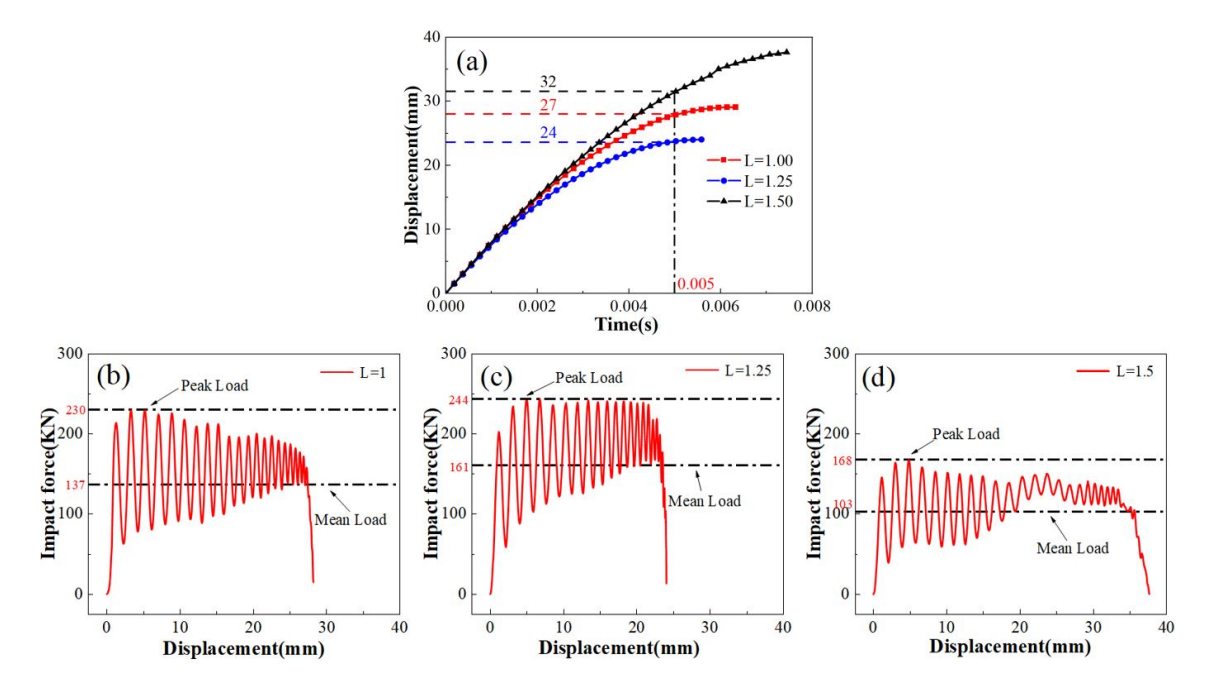
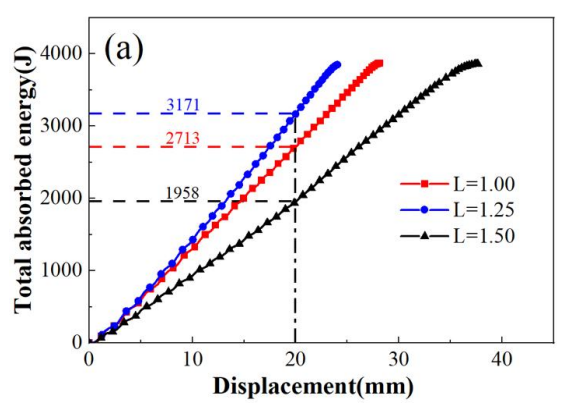


Figure 11 Effect of L on deformation displacement and impact force of AFSDTs: (a) displacement-time curves; (b-d) impact force-displacement curves

The effect of L on the energy absorption performance of IFAFSDTs is presented in Figure 12. As L increases, the total absorbed energy and energy absorption capacity first increase and then decrease. When axial displacement is 20.0 mm, specimens with L of 1, 1.25 and 1.5 exhibited total impact energy absorption values of 2713 J, 3171 J and 1958 J respectively. The energy absorption capacities with strain of 0.3 were measured as 35.7 MJ/m³, 43.3 MJ/m³ and 27.6 MJ/m³. IFAFSDTs with L of 1.25 exhibited superior energy absorption performance. But IFAFSDTs with L of 1.5 exhibit longer energy absorption stroke. As illustrated in Figure 11 (b),

IFAFSDTs with L=1.5 experienced a strain of only 0.42 after impact process. This relatively limited strain resulted in a low degree of densification of the internal foam during deformation, consequently reducing the influence of aluminum foam densification on the overall energy absorption performance of IFAFSDTs [52]. Hence, IFAFSDTs with higher L have greater energy absorption potential. Reducing L will increase the energy absorption of the IFAFSDTs, but at the same time it will reduce its energy absorption stroke, stress will rise sharply, which is not conducive to structural protection [53].



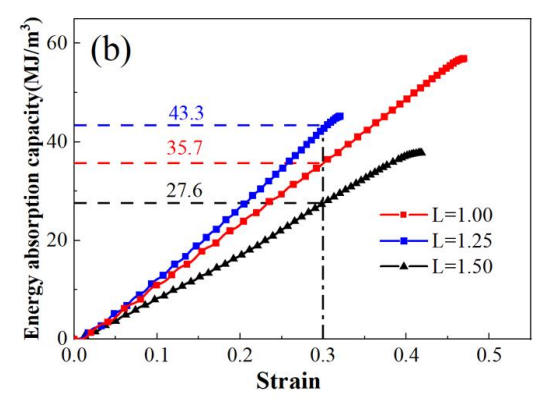


Figure 12 Effect of L on energy absorption performance of IFAFSDTs: (a) total energy absorption; (b) energy absorption capacity.

The effect of L on the ULC of IFAFSDTs during drop-weight impact is illustrated in Figure 13 (a). Load fluctuation of IFAFSDTs is high during the initial impact stage and then gradually decreases. Samples with L=1.25 exhibit the least ULC throughout the impact process. The effect of L on the deformation velocity of IFAFSDTs during axial impact is illustrated in Figure13 (b). As L increases, the reduction of velocity first increases and then decreases. With axial deformation displacement of 20.0 mm, the deformation velocity for the three specimens are 5.20 m/s, 3.50 m/s and 6.20 m/s, respectively, representing reductions of 41.2%, 60.1% and 29.9% from the initial

velocity. The effect of L on the deformation acceleration of IFAFSDTs is shown in Figure 13 (c). When IFAFSDTs subjected to impact, the deformation acceleration will rise rapidly to a certain value and then fluctuate at a higher level and a lower amplitude, indicates that these samples all have a stable buffering process [44]. Specimens with L=1.25 exhibited the highest deformation acceleration, indicating superior crashworthiness. However, excessively high deformation acceleration may pose a risk due to inertial effects, causing the protected individual to experience significant velocity change in a short period of time and potentially resulting in injury [54].

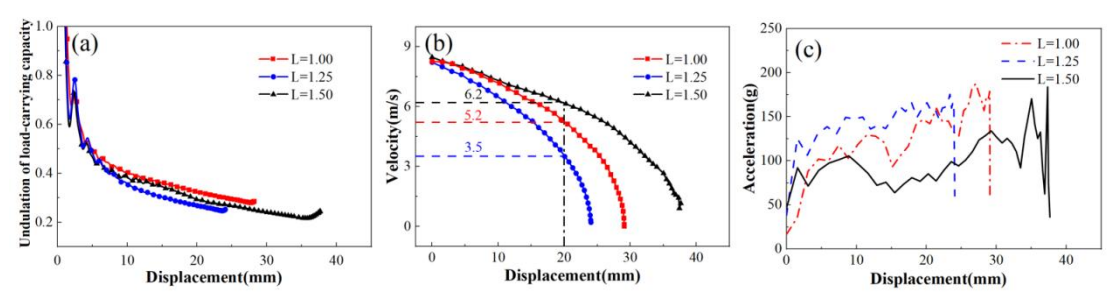


Figure 13 Effect of L on crashworthiness of IFAFSDTs:(a) undulation of load-carrying capacity; (b) deformation velocity; (c) deformation acceleration.

3.5 Deformation and failure mechanism

In order to enhance the impact performance and protection capability of IFAFSDTs, this work investigated deformation and failure mechanisms of IFAFSDTs with different R and L under axial impact loading. When drop hammer contacts with the specimen, one end of IFAFSDTs initially undergoes buckling deformation. As impact process progresses, the other end also experiences the same type of deformation. Finally, non-axisymmetric buckling deformation occurs in middle section of the sample. Under high-speed impact, the Plateau boundaries of aluminum foam core gradually collapse and fracture, resulting in IFAFSDTs being compacted [55]. The filling of aluminum foam can reduce the maximum axial displacement of IFAFSDTs, enhance the overall energy absorption capacity, and prevent a sharp increase in impact force when the sandwich tubes reach densification [56]. The interaction between the aluminum foam core and the solid aluminum tubes also significantly improves the impact performance of IFAFSDTs [57]. Compared to CAFTs reported in previous work of the same dimensions [27], the deformation and damage extent of IFAFSDTs under drop hammer impact are lower, and their impact resistance is superior. This is attributed to the metallurgical bonding between the sandwich core and inner/outer aluminum alloy tubes, which enhances the overall deformation resistance and stiffness [58, 59]. Additionally, the inner tube provides strong lateral constraints, effectively suppressing the deformation of the overall structure. The addition of inner tube improves the axial impact resistance and energy absorption performance of the aluminum foam-filled tube structure, effectively stabilizes its deformation mode, and makes the energy absorption and impact resistance processes more stable [60].

For a given height of IFAFSDTs, the buckling deformation of IFAFSDTs with low R values under

drop hammer impact initially occurs near the impact end. Subsequently, impact stress is transmitted through foam core and solid double tubes to the base plate. Under the reaction force of the base plate, buckling deformation occurs at the bottom of the IFAFSDTs, further absorbing the kinetic energy of the drop hammer. As drop hammer continues to move, the deformation of the IFAFSDTs increases, and the volume decreases during impact process. Fragments generated during the densification of the sandwich core and the deformed regions move radially along the tube [18], forming buckling in the middle section of IFAFSDTs, as shown in Figure 14. At elevated R values, the volume of the solid aluminum tube increases. Due to the fast transmission of stress waves in high-density aluminum alloy tube [61], the impact load is rapidly transmitted through the solid aluminum tubes to the bottom of the IFAFSDTs, leading to the initial formation of buckling deformation near the base plate, followed by the formation of wrinkles in the upper and middle sections, as shown in Figure 14 (c). Due to the varying degrees of densification in different regions of the aluminum foam core during compression, the resulting wrinkles are not perfectly symmetrical rings. Both inner and outer tubes exhibit buckling deformation. The deformation degree of the inner tube is greater, and cracks appear at the folds. This indicates that the inner tube bears a significant portion of the impact load, effectively enhancing the overall impact resistance of the structure [57]. When R=0.25, the wrinkles in the middle section of the specimen are not pronounced, suggesting that a higher filling of aluminum foam suppresses the buckling deformation of the outer tube of the IFAFSDTs. When R=0.35, localized cracks appear in the outer tube of the specimen. Combined with experimental data, it is observed that the peak impact load and average stress are higher at R=0.35, which is the cause of the crack formation.

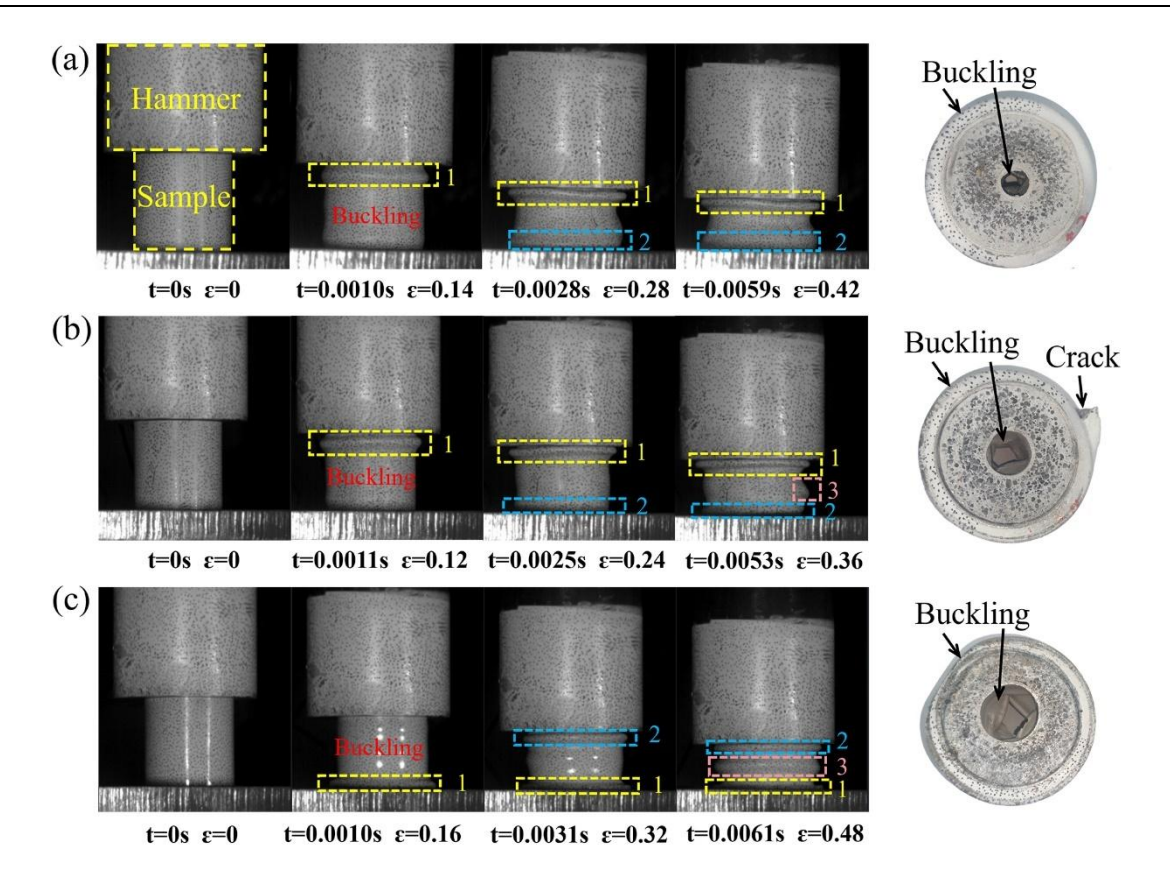


Figure 14 Impact process and failure mode of IFAFSDTs with different R: (a) R=0.25; (b) R=0.35; (c) R=0.45.

The impact velocity of the drop hammer contacting samples with L of 1 is relatively high, leading to localized crushing on the upper surface of the specimen. When the diameter of inner tube remains constant and L increases from 1 to 1.25, the buckling deformation mode of IFAFSDTs transitions from initial buckling at the bottom to nearly simultaneous buckling at both the top and bottom, as shown in Figure 15. This indicates that an increase in the height of IFAFSDTs enhances the plasticity and deformation capacity of the structure. The stress wave is rapidly transmitted through the solid aluminum alloy tube to the bottom plate, and the reaction force from the bottom plate causes buckling deformation in the lower part of the tube. When the height of the IFAFSDTs is further increased to L=1.5, the time for the stress wave to reach the bottom becomes longer. And due to the inertial effect, the aluminum foam core and aluminum alloy tube at the impact end yield first, while the support end undergoes plastic deformation initially until the stress wave propagates to the support end [62]. Therefore, the position where buckling deformation first occurs is related to the filling amount of aluminum foam, inertia effect and stress wave

transmission speed [63].

In conclusion, the outer tube of IFAFSDTs shows an axisymmetric circular buckling deformation mode, which exhibits high energy absorption efficiency [64]. This is attributed to the restriction of inward lateral displacement by the aluminum foam core and inner tube, ensuring the stability of the outer tube deformation [17]. The inner tube without central filler support undergoes severe wall deformation under drop hammer impact, with folds compressing against each other leading to cracks. The inner tube exhibits an asymmetric diamond mode. The deformation of the aluminum foam core is constrained by both the inner and outer tubes, absorbing energy through a densification process under impact stress and providing support to the outer tube. Compared to FFTs and CAFTs, the metallurgical bonding between the aluminum foam core and the inner/outer tubes in IFAFSDTs results in more significant interactions between the core layer and the tube walls [65], which endows IFAFSDTs with superior energy absorption performance under identical drop hammer impact conditions.

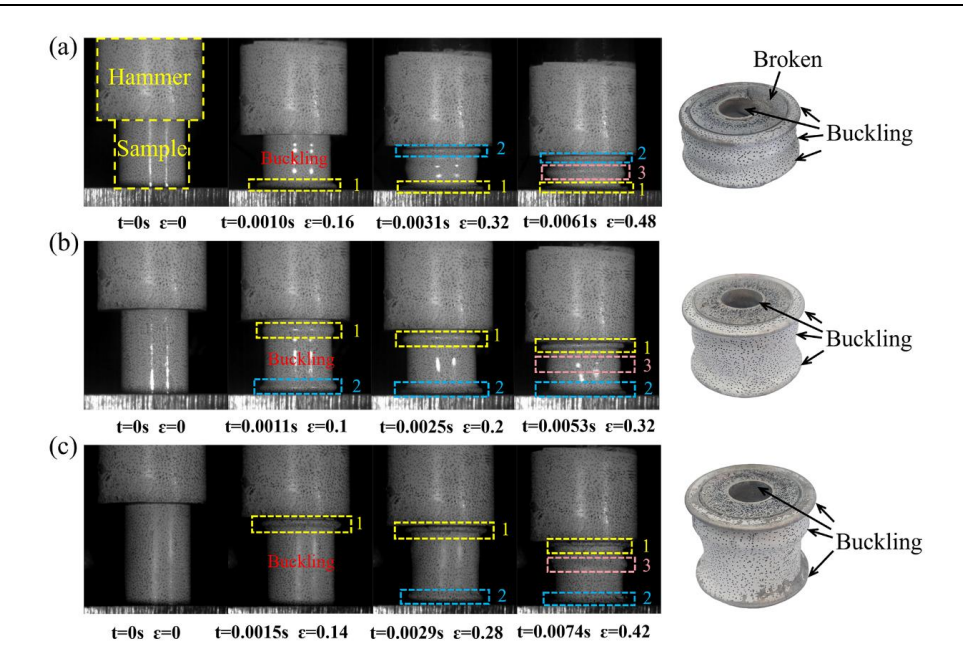


Figure 15 Impact process and failure mode of IFAFSDTs with different L: (a) L=1.0; (b) L=1.25; (c) L=1.5

To further investigate the deformation and failure mechanism of AFSDTs, FE simulation was conducted on the drop-weight impact process. Simulation results were in good agreement with experimental results, as shown in Figure 16. From stress cloud map, during initial deformation process, the impact end is subjected to a large impact force, the stress is mainly concentrated on the inner and outer tube, while aluminum foam core has no obvious deformation. Then obvious buckling deformation appears under 0.25 strain. From simulation results, the stress on inner and outer tubes further increases, and foam core near

第 17 届亚洲铸造会议

impact end has obvious deformation and cracks appear on some cell walls. When strain is 0.375, the sample has axisymmetric and non-axisymmetric circular folds. The non-axisymmetric circular fold is caused by local inhomogeneity of aluminum foam core. Cracks appear in both inner and outer tubes. The foam core has a large degree of deformation and stress concentration with some cell walls broken. When strain reaches 0.5, the sample forms a collapse zone along the stress concentration and fracture site of the inner tube. And the inner/outer tubes further fracture, resulting in the overall failure [66].

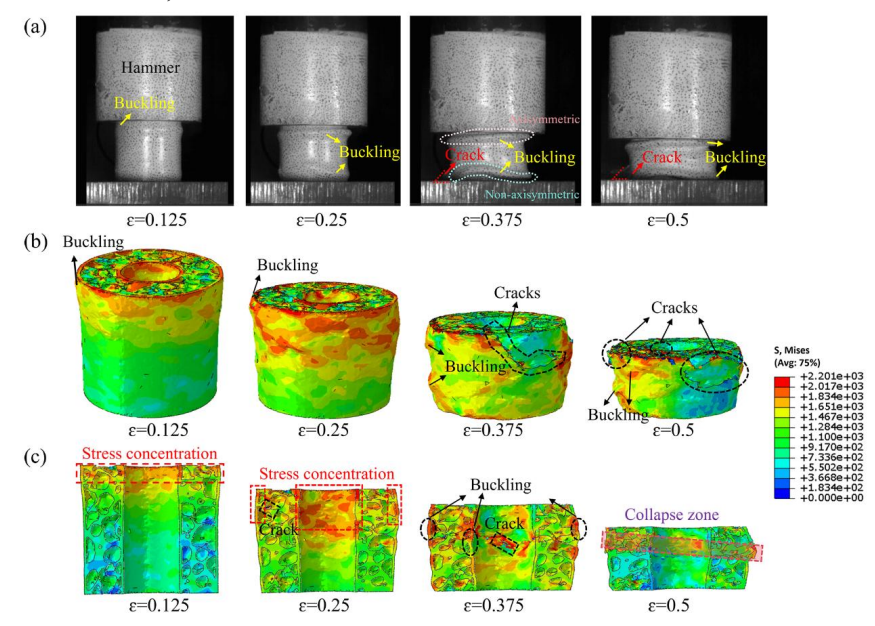


Figure 16 Deformation and failure mechanism of IFAFSDTs: (a) experimental impact process; (b)(c) stress cloud map.

3.6 Energy absorption forms during drop weight impact process

IFAFSDTs prepared by the integrated forming method are different in the energy absorption mode from those prepared by placing the foam core directly into alloy tube [25, 67] or bonding the foam core to the alloy tube [68, 69]. This is due to the high bonding strength of metallurgical bonding interface, which contributes to improve energy absorption efficiency [70]. The energy absorption mechanism of IFAFSDTs in impact process is manifested in the following four forms: (1) energy absorption of outer tube through the axisymmetric buckling deformation mode; (2) energy absorption of inner tube through diamond deformation mode; (3) energy absorption of aluminum foam core through deformation, disruption and densification; (4) energy absorption through the damage and tearing of the metallurgical bonding interface between aluminum foam core and inner/outer tubes. Through SEM analysis (sampling positions are shown in Figure 17(c)), the microscopic energy absorption mechanism of aluminum foam core can be further divided into three forms: (1) energy absorbed through deformation and collapse of cells, while the initiation and propagation of cracks around collapsed cells further enhance energy dissipation; (2) energy absorption via deformation, manifested by the grain plastic elongation of grains along a specific direction; (3) partial areas inside the nodes and cell walls absorb

energy through the intergranular fracture mechanism.

In regions with different degrees of deformation, energy absorption mechanisms microstructures show significant differences. At the impact and support ends of IFAFSDTs, the collapse of cell walls leads to the interconnection of adjacent cells (Figure 17(a)(b)), and the densification of the aluminum foam core absorbs impact energy. Cells are strongly compressed and accompanied by crack formation in the severely deformed regions such as impact end, support end and the extruded region of the aluminum alloy tube (Figure 17(d)). Due to the coordinated effect of polycrystalline deformation, grains around collapsed cells undergo significant elongation along the compression direction. In the middle area of IFAFSDTs, the deformation of foam aluminum is relatively mild, cells are relatively complete. Grains near the walls of aluminum alloy tube and at the nodes have no obvious deformation, and only local microcracks distributed along the grain boundary rarely penetrate the grains (Figure 17(e)). In the transition region between the two ends and the middle is a medium deformation area, and grains near the wall of tube and at nodes are elongated in different directions (Figure 17(f) and (g)). The grains in the lower middle region are elongated in the upper left-bottom right direction (blue solid line box), and the grains in the lower region are elongated in the lower left-upper right direction (green dashed line box).

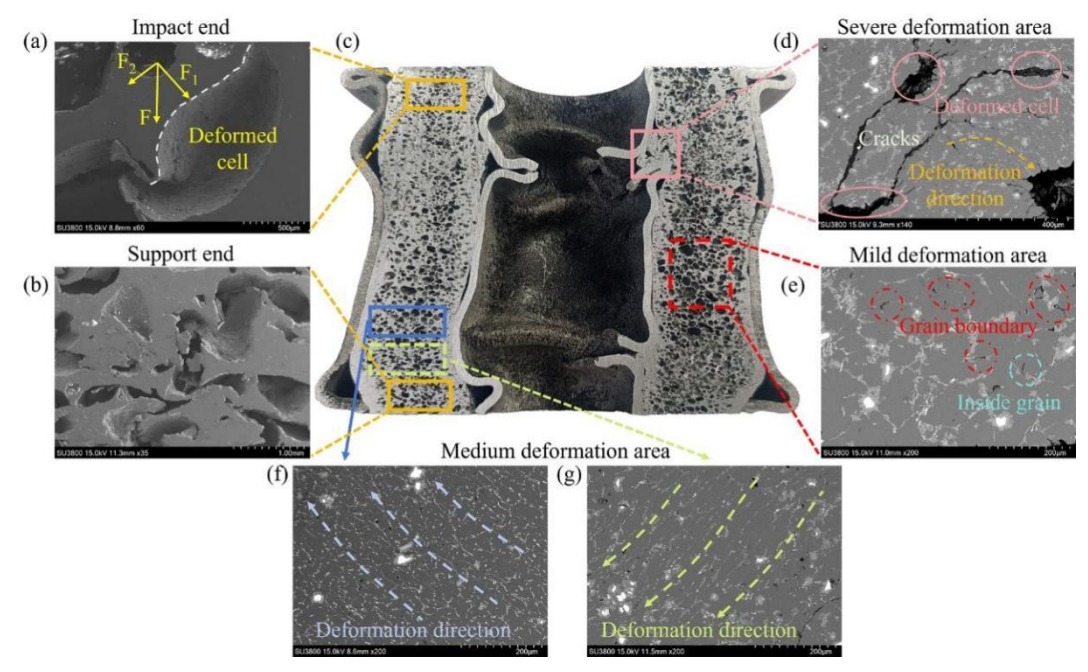
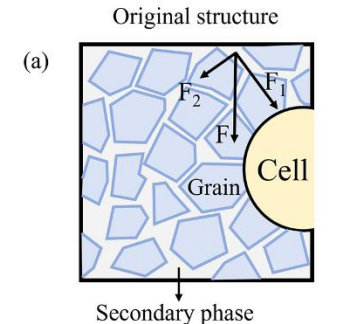
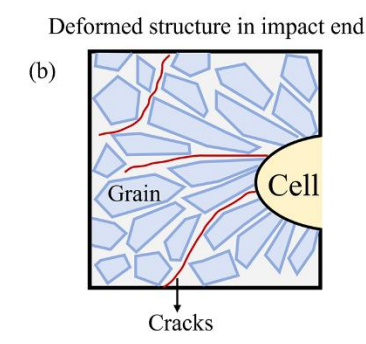


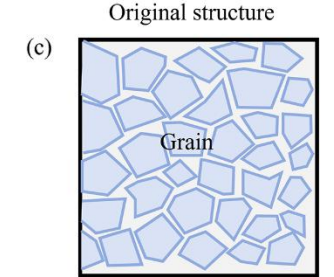
Figure 17 Microstructures of aluminum foam core after impact: (a) impact end; (b) support end; (c) sampling positions; (d) large deformation area; (e) mild deformation area; (f)(g) medium deformation area

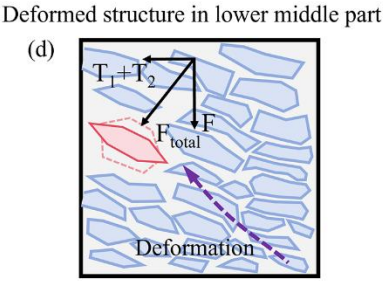
To further explain the grain deformation and crack propagation mechanism in aluminum foam core, the forces applied to different regions of the foam core were analyzed. Taking the impact end as an example (Figure 18(a)), the vertical impact force F can be decomposed into F₁ and F₂. F₁ drives the deformation of the cells and elongates the surrounding grains along the direction of deformation (Figure 18(b)). F₂ causes the initiation and propagation of cracks along the second phase at the grain boundaries. In the region of medium deformation, the deformation behavior exhibits significant regional differences. Due to metallurgical bonding at the interface, the buckling deformation of the outer tube drives the aluminum foam at the wall outward along the diameter. When the inner tube is impacted, it will deform inwards and outwards at the same time. When it deforms inwards, the metallurgical bonding interface is easy to be damaged, which makes aluminum foam core and the inner tube separated. When deformed outwards, inner tube and aluminum foam core are better bonded and will push aluminum foam outwards. Therefore, in the lower middle region (Figure 18(d)), the combined force F of the impact and support force together with the inner and outer tube forces (T₁ from the outer tube buckling and T₂ generated by the inner tube deformation) form F_{total}, causing grains to elongate in a specific direction. In the lower part of IFAFSDTs, the support force is larger and the combined force in the vertical direction is N. Under the combined effect of N, T₁ and T₂, grains elongate along the deformation direction shown in Figure 18(e). Therefore, the difference in deformation modes of aluminum foam core mainly depends on the dynamic balance between impact force and support force, the synergy of deformation behavior of inner and outer tube, and the bonding strength of metallurgical bonding interface. These factors collectively determine the energy absorbing properties of aluminum foam core.





(e)





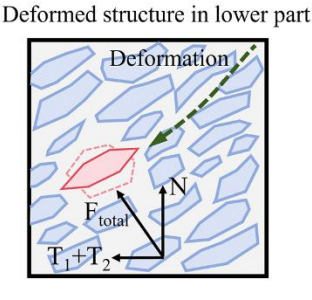


Figure 18 Grain deformation and crack propagation mechanism: (a) original structure and force analysis in impact end; (b) deformed structure in impact end; (c) original structure in medium deformation area; (d) deformed structure and force analysis in lower middle part;

(e) deformed structure and force analysis in lower part.

Subsequently, the three energy absorption mechanisms of aluminum foam core under dynamic impact (energy absorption through wall deformation and collapse, accompanied by the formation of cracks, grain deformation intergranular fracture) were quantitatively evaluated. The energy absorbed by cell wall deformation and collapse (W_{cell}) is calculated by Gibson-Ashby foam material theory combined with unit cell model [71, 72], and the dynamic enhancement factor $C(\dot{\varepsilon})$ was used to characterize the strain rate effect ^[73], which is calibrated through drop-weight hammer impact test. For the energy absorption mechanism of grain plastic deformation, based on the theory of dislocation energy storage ^[74], the energy absorbed during grain elongation (W_{disl}) is quantified by calculating the dislocation density after deformation. This energy is mainly converted into grain boundary slip or rotation,

dislocation proliferation and movement, and lattice elastic energy storage $^{[75, 76]}$. The energy absorbed by intergranular fracture (W_{GB}) depends on the fracture surface energy and grain boundary characteristics $^{[77]}$. The key parameters, average grain size D and intergranular fracture ratio f_{GB} , were obtained through statistical analysis of SEM images using Image J software.

$$W_{cell} = \sigma_{\nu} \varepsilon_{p} (1 - P) C(\dot{\varepsilon}) \tag{10}$$

$$W_{disl} = \frac{1}{2}Gb^2\rho \tag{11}$$

$$W_{GB} = \gamma A_{GB} C(\dot{\varepsilon}) f_{GB} / V \tag{12}$$

where σ_y is the yield strength of the matrix alloy, ε_p represents the densification strain of the foam core, P is porosity, G is the matrix shear modulus, b is the Burgers vector, ρ denotes the dislocation density of the deformed foam aluminum, γ_{GB} is the grain

boundary fracture energy per unit area. According to Griffth's theory, the relationship between the fracture energy γ and the surface energy γ_s and grain boundary energy γ_{GB} can be expressed as: $\gamma = 2\gamma_s - \gamma_{GB}$ [78, 79]. A_{GB} is the total area of fractured grain boundaries, f_{GB} is the proportion of intergranular fracture, and V represents the volume of intergranular fracture.

Based on existing literature reports and experimental data, the relevant parameters were obtained. The parameters are listed in Table 2, and the dislocation density is taken as 10¹⁵ for calculation. The energy absorption capabilities of three mechanisms: cell wall deformation and collapse, grain deformation and grain boundary fracture were compared and quantified, as shown in Figure 19. It can be seen that the deformation and collapse of the cell wall is the main source of energy absorption of aluminum foam core.

Table. 2 Parameters used for calculating energy absorption

$\sigma_y(MPa)$	$arepsilon_p$	$\mathcal{C}(\dot{\varepsilon})$	G(GPa)	b(nm)	$\rho(\mathrm{m}^{-2})$	$\gamma(J/m^2)$	$D(\mu m)$	f_{GB}
82.354 [42]	0.42	3.6	27[80]	0.286	10 ¹⁴ ~10 ¹⁶ [81]	1.9 [78]	45.8	0.2

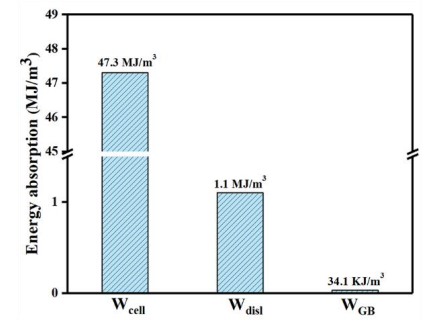


Figure 19 Energy absorption capacity of different energy absorption mechanisms in aluminum foam core.

4. Conclusions

This paper employed the improved melt foaming method to accomplish the integral preparation of IFAFSDTs. The axial impact resistance of IFAFSDTs was systematically evaluated through drop weight impact testing, with particular emphasis on the effect of R and L. Furthermore, deformation characteristics and failure mechanisms of IFAFSDTs were analyzed, and principal findings of this work can be summarized as follows:

(1) IFAFSDTs with metallurgical bonding between the aluminum foam core and inner/outer aluminum alloy tubes were fabricated using integrated forming method. Inner/outer tubes maintain their structural integrity without deformation, while the aluminum foam core exhibits a uniform pore structure distribution.

- (2) The load-carrying capacity and energy absorption performance of IFAFSDTs increase first and then decrease with the increase of *R* and *L*. IFAFSDTs with high *R* or *L* value exhibit relatively stable load fluctuations during the impact process, and the deformation acceleration and impact stress are lower. Hence, appropriately increasing the inner tube diameter and the sample height constitutes an efficacious approach to further enhance the axial impact resistance of IFAFSDTs and stabilize their energy absorption process.
- (3) Compared with CAFTs reported previously, IFAFSDTs demonstrate superior energy absorption capacity and enhanced resistance to axial deformation. During impact process, outer aluminum alloy tube exhibits an axisymmetric circular progressive buckling deformation mode, while inner tube follows an asymmetric diamond mode, aluminum foam core undergoes the densification process, and metallurgical bonding interface is damaged. There is a strong interaction between aluminum foam core and inner/outer tubes, effectively constraining excessive deformation of the tubes. Furthermore, the sequence and location of buckling deformation and wrinkling formation are influenced by multiple factors, including the filling amount of aluminum foam, inertia effect and stress wave transmission speed.

(4) Aluminum foam core absorbs impact energy of falling weight through modes of pore structure deformation, crack propagation and grain deformation. The differences in the energy absorption modes mainly depend on the dynamic balance between the impact and the support force, the deformation behavior of the inner and outer tubes and the bonding strength of the metallurgical interface. This leads to different energy absorption modes and microstructures after deformation at different positions.

Data Availability

Data will be made available on request.

Acknowledgement

This work was supported financially by Hebei Provincial General Natural Science Foundation Project (No.:2025202207), Civil-Military Science and Technology Collaborative Innovation Special Project (No.: 22351003D), Central Guidance Local Science and Project Technology Development Fund (No.: 246Z1029G) and the Hebei Province Higher Education Science Technology Research Project (No.: ZD2020191).

Conflict of Interest

No conflict of interest and dedication statement exists in the submission of this manuscript.

References

- [1] Zhao C, Zhong J, Wang H, et al. Impact behaviour and protection performance of a CFRP NPR skeleton filled with aluminum foam[J]. Mater. Design. 2024; 246: 113295.
- [2] Wattad O and Grisaro H Y. On the efficiency of uniform aluminum foam as energy-absorbing sacrificial cladding for structural blast mitigation[J]. Int. J. Mech. Sci. 2024; 308: 118047.
- [3] Zhang Z, Feng H, Xu T, et al. Compression performances of integral-forming aluminum foam sandwich[J]. Compos. Struct. 2022; 283: 115090.
- [4] Yi Z, Si-Yuan H, Jia-Gui L, et al. Density gradient tailoring of aluminum foam-filled tube. Compos. Struct. 2019; 220: 451-459.
- [5] Song J, Xu S, Xu L, et al. Experimental study on the crashworthiness of bio-inspired aluminum foam-filled tubes under axial compression loading[J]. Thin. Wall. Struct. 2020; 155: 106937.
- [6] Mirbagheri S M H and Salehi M. Complementary and normalized energies during static and dynamic uniaxial deformation of single and multi-layer foam-filled tube[J]. J. Sandw. Struct. Mater. 2022; 24:1470-1490.
- [7] Salehi M, Mirbagheri S, Ramiani A J. Efficient energy

- absorption of functionally-graded metallic foam-filled tubes under impact loading[J]. T. Nonferr. Metal. Soc. 2021; 31(1): 92-110.
- [8] Movahedi N and Linul E. Quasi-static compressive behavior of the ex-situ aluminum-alloy foam-filled tubes under elevated temperature conditions[J]. Mater. Lett. 2017; 206: 182-184.
- [9] Li Z, Yu J, Guo L. Deformation and energy absorption of aluminum foam-filled tubes subjected to oblique loading[J]. Int. J. Mech. Sci. 2012; 54(1): 48-56.
- [10] Sun G, Chen D, Wang H, et al. High-velocity impact behaviour of aluminium honeycomb sandwich panels with different structural configurations[J]. Int. J. Impact. Eng. 2018; 122: 119-136.
- [11] Gao X, Zhang M, Huang Y, et al. Experimental and numerical investigation of thermoplastic honeycomb sandwich structures under bending loading[J]. Thin. Wall. Struct. 2020; 155: 106961.
- [12] Jafarian B and Rezvani M J. An experimental investigation on energy absorption of thin-walled bitubal structures by inversion and axial collapse[J]. Int. J. Mech. Sci. 2017; 126: 270-280.
- [13] Sun G, Wang Z, Yu H, et al. Experimental and numerical investigation into the crashworthiness of metal-foam-composite hybrid structures[J]. Compos. Struct. 2019; 209: 535-547.
- [14] Linul E and Khezrzadeh O. Axial crashworthiness performance of foam-based composite structures under extreme temperature conditions[J]. Compos. Struct. 2021; 271: 114156.
- [15] Garai F, Beres G, Weltsch Z. Development of tubes filled with aluminium foams for lightweight vehicle manufacturing[J]. Mat. Sci. Eng. A. 2020; 790: 139743.
- [16] Rogala M, Ferdynus M, Gawdzi ń ska K, et al. The influence of different length aluminum foam filling on mechanical behavior of a square thin-walled column[J]. Materials. 2021; 14(13): 3630.
- [17] Duarte I, Krstulović-Opara L, Vesenjak M. Axial crush behaviour of the aluminium alloy in-situ foam filled tubes with very low wall thickness[J]. Compos. Struct. 2018; 192: 184-192.
- [18] Hangai Y, Otazawa S, Utsunomiya T. Aluminum alloy foam-filled aluminum tube fabricated by friction stir back extrusion and its compression properties[J]. Compos. Struct. 2018; 183: 416-422.
- [19] Taherishargh M, Vesenjak M, Belova I, et al. In situ manufacturing and mechanical properties of syntactic foam filled tubes[J]. Mater. Design. 2016; 99: 356-368.
- [20] Chen Y, Hou S, Fu K, et al. Low-velocity impact

- response of composite sandwich structures: modelling and experiment[J]. Compos. Struct. 2017; 168: 322-334.
- [21] Tarlochan F, Ramesh S, Harpreet S. Advanced composite sandwich structure design for energy absorption applications: Blast protection and crashworthiness[J]. Compos. Part B-Eng. 2012; 43(5): 2198-2208.
- [22] Wang Y, Zhang R, Liu S, et al. Energy absorption behaviour of an aluminium foam-filled circular-triangular nested tube energy absorber under impact loading. Structures[J]. 2021; 34: 95-104.
- [23] Guo L and Yu J. Dynamic bending response of double cylindrical tubes filled with aluminum foam[J]. Int. J. Impact. Eng. 2011; 38(2): 85-94.
- [24] Ni X H, Zhang X G, Han D, et al. Aluminum foam-filled auxetic double tubular structures: design and characteristic study[J]. Mech. Adv. Mater. Struc. 2024; 31(15): 3377-3388.
- [25] Yan S, Jiang Y, Deng Y, et al. Energy absorption characteristics of aluminum foam-filled corrugated tube under axial compression loading[J]. Thin. Wall. Struct. 2024; 195: 111333.
- [26] Duarte I, Vesenjak M, Krstulović-Opara L, et al. Manufacturing and bending behaviour of in situ foam-filled aluminium alloy tubes[J]. Mater. Design. 2015; 66: 532-544.
- [27] Wang J, Xu X, Zhang Z, et al. Axial Impact Performances of Composite Aluminum Foam Tubes[J]. Adv. Eng. Mater. 2024; 26(20): 2400897.
- [28] San Ha N and Lu G. A review of recent research on bio-inspired structures and materials for energy absorption applications[J]. Compos. Part B-Eng. 2020; 181: 107496.
- [29] San Ha N, Pham T M, Tran T T, et al. Mechanical properties and energy absorption of bio-inspired hierarchical circular honeycomb[J]. Compos. Part B-Eng. 2022; 236: 109818.
- [30] Wang W, Wang Y, Zhao Z, et al. Numerical simulation and experimental study on energy absorption of foam-filled local nanocrystallized thin-walled tubes under axial crushing [J]. Materials. 2022; 15(16): 5556.
- [31] Xie S, Zhang J, Liu X, et al. A reinforced energy-absorbing structure formed by combining multiple aluminum foam-filled open-hole tubes[J]. Int. J. Mech. Sci. 2022: 224.
- [32] Hu H, Lai Z, Ding G. Influence of surface wettability on heat transfer and pressure drop characteristics of wet air in metal foam under dehumidifying conditions[J]. Int. J. Therm. Sci. 2019; 135: 331-343.
- [33] Wang N, Chen X, Maire E, et al. Study on Cell

- Deformation of Low Porosity Aluminum Foams under Quasi Static Compression by X Ray Tomography[J]. Adv. Eng. Mater. 2020; 22(10): 2000264.
- [34] Kim S, Choi S, Ahn T Y, et al. Effect of Space Holder Size on Microstructure and Mechanical Properties of Aluminum Foam[J]. Met. Mater. Int. 2025; 1-11.
- [35] Çıbıkçı K Ç and Yaman M. Experimental investigation of compressive behavior and vibration properties of layered hybrid foam formed by aluminum foam/EPS-filled syntactic foam[J]. J. Mater. Sci. 2024; 59(8): 3636-3651.
- [36] Liu N, Zhang Z, Xia X, et al. Local deformation on damping performance of integral-forming aluminum foam sandwich[J]. Mater. Lett. 2022; 323: 132545.
- [37] Zhang Z, Zhang Z, Liu N, et al. Three-point bending performances of integral-forming aluminum foam sandwich[J]. Mater. Design. 2023; 229: 111889.
- [38] Mohan K, Yip T H, Idapalapati S, et al. Impact response of aluminum foam core sandwich structures[J]. Mat. Sci. Eng. A. 2011; 529: 94-101.
- [39] Zhang Y, Liu Q, He Z, et al. Dynamic impact response of aluminum honeycombs filled with Expanded Polypropylene foam[J]. Compos. Part. B-Eng. 2019; 156: 17-27.
- [40] Yamashita M and Gotoh M. Impact behavior of honeycomb structures with various cell specifications numerical simulation and experiment[J]. Int. J. Impact Eng. 2005; 32(1): 618-630.
- [41] Duarte I, Vesenjak M, Krstulović-Opara L. Variation of quasi-static and dynamic compressive properties in a single aluminium foam block[J]. Mat. Sci. Eng. A. 2014; 616: 171-182.
- [42] Zhang Z, Liu N, Zhang Z, et al. Compression performances of composite aluminum foam tubes[J]. Int. J. Mech. Sci. 2023; 242: 108039.
- [43] Sun G, Li S, Liu Q, et al. Experimental study on crashworthiness of empty/aluminum foam/honeycomb-filled CFRP tubes[J]. Compos. Struct. 2016; 152: 969-993.
- [44] Yang H, Lei H, Lu G. Crashworthiness of circular fiber reinforced plastic tubes filled with composite skeletons/aluminum foam under drop-weight impact loading[J]. Thin. Wall. Struct. 2021; 160: 107380.
- [45] Linul E, Movahedi N, Marsavina L. The temperature effect on the axial quasi-static compressive behavior of ex-situ aluminum foam-filled tubes[J]. Compos. Struct. 2017; 180: 709-722.
- [46] Kao Y-T, Amin A R, Payne N, et al. Low-velocity impact response of 3D-printed lattice structure with foam reinforcement[J]. Compos. Struct. 2018; 192: 93-100.

- [47] Kim S, Kim D G, Kim M, et al. Analyses of impact energy-absorbing performance of open-and closed-cell Al foams using modified split Hopkinson pressure bar[J]. J. Alloy. Compd. 2023; 965: 171349.
- [48] Zhang Y, Sun L, Ren X, et al. Design and analysis of an auxetic metamaterial with tuneable stiffness[J]. Compos. Struct. 2022; 281: 114997.
- [49] Abdulqadir S, Alaseel B, Ansari M. Simulation of thin-walled double hexagonal aluminium 5754 alloy foam-filled section subjected to direct and oblique loading[J]. Mater. Today. 2021; 42: 2822-2828.
- [50] Djamaluddin F, Abdullah S, Ariffin A, et al. Optimization of foam-filled double circular tubes under axial and oblique impact loading conditions[J]. Thin. Wall. Struct. 2015; 87: 1-11.
- [51] Jensen Ø and Langseth M, Hopperstad O. Experimental investigations on the behaviour of short to long square aluminium tubes subjected to axial loading[J]. Int. J. Impact. Eng. 2004; 30(8): 973-1003.
- [52] Saleem F, Li S, Cui S, et al. The strain rate and density dependence of the mechanical properties of closed-cell aluminum foam[J]. Mat. Sci. Eng. A. 2023; 884: 145568.
- [53] Xiang Y, Wang M, Yu T, et al. Key performance indicators of tubes and foam-filled tubes used as energy absorbers[J]. Int. J. Appl. Mech. 2015; 7(4): 1550060.
- [54] Reid J D, Hascall J A, Sicking D L, et al. Inertial effects during impact testing[J]. Transport. Res. Rec. 2009; 2120(1): 39-46.
- [55] Zhang J, Chen L, Wu H, et al. Experimental and mesoscopic investigation of double-layer aluminum foam under impact loading[J]. Compos. Struct. 2020; 241: 110859.
- [56] Lu J, Wang Y, Zhai X, et al. Impact behavior of a cladding sandwich panel with aluminum foam-filled tubular cores[J]. Thin. Wall. Struct. 2021; 169: 108459.
- [57] Li S, Guo X, Liao J, et al. Crushing analysis and design optimization for foam-filled aluminum/CFRP hybrid tube against transverse impact[J]. Compos. Part B-Eng. 2020; 196: 108029.
- [58] Zhang K, Zhu X, Wang R, et al. Structural performance of aluminum foam-filled multi-cell steel tubes under axial impact[J]. Structures. 2024: 107527.
- [59] Li X, Yin Y, Zhu X, et al. Performance of hollow and aluminum foam-filled multi-cell thin-walled aluminum alloy tubes (6063-T5) under axial impact[J]. Structures. 2023: 1803.
- [60] Meng L, Zhai X, Wang Y. Investigation on lateral impact resistant performance of aluminum foam-filled 6082-T6 aluminum alloy circular tubes: Experimental and

- numerical study[J]. Thin. Wall. Struct. 2023; 188: 110816.
- [61] Wang X, Yuan M, Miao Y, et al. Stress wave propagation characteristics and impact resistance of laminated composites under impact loading[J]. Mech. Adv. Mater. Struc. 2024; 31(8): 1822.
- [62] Duan Y, Chen X, Du B, et al. A predictive model for strain hardening and inertia effect of aluminum tubes filled with aluminum foam[J]. Compos. Struct. 2022; 300: 116177.
- [63] Movahedi N, Fiedler T, Taşdemirci A, et al. Impact loading of functionally graded metal syntactic foams[J]. Mat. Sci. Eng. A. 2022; 839: 142831.
- [64] Fyllingen Ø, Langmoen E, Langseth M, et al. Transition from progressive buckling to global bending of square aluminium tubes[J]. Int. J. Impact. Eng. 2012; 48: 24-32.
- [65] Duarte I, Krstulović-Opara L, Vesenjak M. Characterisation of aluminium alloy tubes filled with aluminium alloy integral-skin foam under axial compressive loads[J]. Compos. Struct. 2015; 121: 154-162.
- [66] Sahu S, Reddy T, Reddy G, et al. Low-velocity impact indentation rate sensitivity of aluminium foams[J]. Mater. Today. Commun. 2020; 24: 101351.
- [67] Zhuang W, Wang E, Zhang D, et al. Mesoscale study on the mechanical properties and energy absorption characteristics of aluminum foam-filled CFRP tubes under axial compression[J]. Mech. Adv. Mater. Struc. 2024; 31: 10330-10346.
- [68] Zhang C J, Yi F, Zhang X. Mechanical properties and energy absorption properties of aluminum foam-filled square tubes[J]. T. Nonferr. Metal. Soc. 2010; 20: 1380-1386.
- [69] Zhang Z, Huang L, Li B, et al. Design of a novel multi-walled tube-reinforced aluminum foam for energy absorption[J]. Compos. Struct. 2021; 276: 114584.
- [70] Meriç D and Gedikli H. Multi-objective optimization of energy absorbing behavior of foam-filled hybrid composite tubes[J]. Compos. Struct. 2022; 279: 114771.
- [71] Hanssen A, Hopperstad O S, Langseth M, et al. Validation of constitutive models applicable to aluminium foams[J]. Int. J. Mech. Sci. 2002; 44(2): 359-406.
- [72] Gibson L J and Ashby M F. Cellular solids: structure and properties[M], 2nd ed. (Cambridge University Press, 1997).
- [73] Deshpande V and Fleck N. High strain rate compressive behaviour of aluminium alloy foams[J]. Int. J. Impact. Eng. 2000; 24: 277.
- [74] Hull D and Bacon D J. Introduction to Dislocations[M],

- 5th ed. (Elsevier, Oxford, 2011).
- [75] Sendrowicz A, Myhre A, Yasnikov I, et al. Stored and dissipated energy of plastic deformation revisited from the viewpoint of dislocation kinetics modelling approach[J]. Acta. Mater. 2022; 237: 118190.
- [76] Chen B, Zhu L, Xin Y, et al. Grain rotation in plastic deformation[J]. Quantum Beam Science. 2019; 3(3): 17.
- [77] Murr L E. Handbook of materials structures, properties, processing and performance[M]. (Springer, Switzerland, 2015).
- [78] Ovid 'Ko I, Sheinerman A, Aifantis E. Stress-driven migration of grain boundaries and fracture processes in

- nanocrystalline ceramics and metals[J]. Acta. Mater. 2008; 56(12): 2718-2727.
- [79] Griffith A A. The phenomena of rupture and flow in solids. Philosophical transactions of the royal society of london[M]. Series A, containing papers of a mathematical or physical character. 1920; 221(4): 163-198.
- [80] Smithells C J. Metals reference book[M], 5th ed. (Elsevier, London, 2013).
- [81] Hughes D and Hansen N. High angle boundaries formed by grain subdivision mechanisms[J]. Acta. Mater. 1997; 45(9): 3871-3886.